in eq 7 are not as easily calculated. A value of -14 cm^3/mol, $\Delta V_{11}^{\ddagger}$, has been calculated for $Co(dmg)_3(BF)_2^{+/0}$ from the study of the pressure dependence of the Co(III) clathrochelate reduction by $FeCp_2$.[18] The value of $\Delta V_{22}^{\ddagger}$ is not available but is constant for the series of reactions. The reaction volume, ΔV^0, is estimated above at 0 to ± 10 cm^3/mol. All of the calculated values for $\Delta V_W^{\ddagger}$ are positive and increase with the size of the clathrochelate. The agreement between just this term and the observed $\Delta V_{12}^{\ddagger}$ for the $Co(nox)_3(BBu)_2$ reaction is good, but the progressively larger complexes have larger volumes of activation than are predicted from $\Delta V_W^{\ddagger}$. The $\Delta V_{11}^{\ddagger}$ is negative, and ΔV^0 is small; thus a constant, positive value for $\Delta V_{22}^{\ddagger}$ could be consistent with the observed pattern.

The volume of activation shows a small dependence on $[BF_4^-]$, with a decrease in $\Delta V^{\ddagger}$ up to ca. 0.05 M added electrolyte. A similar pattern but a larger change is observed for the reactions between the positive Co(III) clathrochelates and ferrocenes.[18] The smaller effect observed here is consistent with the smaller sensitivity of the $Cr(CNdipp)_6^{+/2+}$ reactions to added electrolyte. The remaining effect is not inconsistent with a lack of influence of electrolyte on the rate constant, since an ion-paired path could give the same rate constant and still have a different volume of activation than a free-ion path.

Conclusion

In summary, the experimental cross-reaction rate constants are in good agreement with the predictions from the Marcus cross-reaction relationship. This further supports the values used for the electron self-exchange rate constants. The rate constant is not affected by the presence of added salt. The volumes of activation are positive, ranging from 2.2 to 10.8 cm^3/mol, a result in contrast to all other outer-sphere electron-transfer reactions between reactants that are not oppositely charged.

The unexpected results reported here, the lack of salt dependence at ambient pressure, and the positive volumes of activation, we believe, are related. We suggested that the lack of salt effect was due to the Cr(II) complex. The spherical Cr(II) complex has conjugated ligands which extend the π symmetry orbitals involved in the electron-transfer process, thus giving excellent orbital overlap with the electron acceptor. The presence of an anion does not significantly disturb this overlap. The rate constant decreases with pressure. Although we cannot provide a model with adequate precision to predict this, we believe that it is primarily the solvent release on forming the precursor complex and the reorganized complexes that produces this effect. Since the reactants already have such good orbital overlap, any improvement in the orbital overlap, brought on by a decreased electron-transfer distance accompanying increased pressure, has no effect. This makes us conclude further that the negative volumes of activation and inhibition by ion pairing previously observed occur because these other reactions have inadequate orbital overlap, and this is improved by pressure or further weakened by ion pairing. A similar conclusion about the sensitivity of $\Delta V^{\ddagger}$ to the pressure dependence of the electron-transfer distance has been reached by Swaddle and co-workers from the study of the $MnO_4^{-/2-}$ electron exchange.[31-34,65]

Further work on these problems will be pursued through the study of other reactions of 0/2+ or 0/3+ charge types, and through the study of reactants like the $Cr(CNdipp)_6^{+/2+}$ complexes, but which lack the extensive conjugation. Molar volume studies of the complexes are also being pursued in order to better understand whether the equations being used to estimate molar volumes are adequate and in order to obtain volumes of reaction to use in the calculations.

Acknowledgment. We are pleased to acknowledge helpful discussions with Susan Johns (computer graphics) and Drs. Mark Murguia (data analysis program), Jacqueline Gribble (cobalt synthesis), and Karl Kirchner and Prof. John P. Hunt. This work was supported by the National Science Foundation.

Supplementary Material Available: Tables of second-order rate constant dependence on added electrolyte, concentration, and temperature (15 pages). Ordering information is given on any current masthead page.

(65) (a) Spiccia, L.; Swaddle, T. W. *Inorg. Chem.* **1987**, *26*, 2265. (b) Jolley, W. H.; Stranks, D. R.; Swaddle, T. W. *Inorg. Chem.* **1990**, *29*, 1948.

Contribution from the Department of Chemistry, The University of North Carolina, Chapel Hill, North Carolina 27599-3290

Electrocatalytic Reduction of Nitrite Ion by edta Complexes of Iron(II) and Ruthenium(II)

Matthew R. Rhodes, Mark H. Barley, and Thomas J. Meyer*

Received June 12, 1989

The reductive electrochemistries of both $[Ru^{II}(Hedta)(NO^+)]^0$ and $[Fe^{II}(Hedta)(NO^{\bullet})]^-$ have been investigated as a function of pH. The nitrosyl complexes are effective electrocatalysts for the reduction of NO_2^- or HONO to give the reduced products N_2O, N_2, NH_3OH^+, or NH_4^+. An element of product selectivity is available by making appropriate choices in pH, applied potential, or catalyst. The mechanisms by which nitrite is reduced appear to be similar to those identified earlier for polypyridyl complexes of Ru and Os and for water-soluble porphine complexes of Fe.

Introduction

One of the themes in our current research is an attempt to uncover pathways for the redox transformations of small inorganic molecules or ions such as CO_2/HCO_2H,[1] H_2O/O_2,[2] SO_2/H_2S,[3] or NO_2^-/NH_3.[4-6] The approach that has been taken has been (1) to identify the individual steps by which these multiple electron

(1) (a) Bolinger, C. M.; Story, N.; Sullivan, B. P.; Meyer, T. J. *Inorg. Chem.* **1988**, *27*, 4582. (b) O'Toole, T. R.; Sullivan, B. P.; Bruce, M. R.; Margerum, L. D.; Murray, R. W.; Meyer, T. J. *J. Electroanal. Chem. Interfacial Electrochem.* **1989**, *259*, 217. (c) Bruce, M. R.; Megehee, E.; Sullivan, B. P.; Thorp, H.; O'Toole, T. R.; Downard, A.; Meyer, T. J. *Organometallics* **1988**, *7*, 238. (d) Sullivan, B. P.; Bruce, M. R.; O'Toole, T. R.; Bolinger, C. M.; Megehee, E.; Thorp, H.; Meyer, T. J. In *Catalytic Activation of Carbon Dioxide*; Ayers, W. M., Ed., ACS Symposium Series 363; American Chemical Society: Washington, DC, 1988; Chapter 6, p 52.

(2) (a) Gersten, S. W.; Samuels, G. J.; Meyer, T. J. *J. Am. Chem. Soc.* **1982**, *104*, 4029. (b) Gilbert, J. A.; Eggleston, D. S.; Murphy, W. R.; Geselowitz, D. A.; Gersten, S. W.; Hodgson, D. J.; Meyer, T. J. *J. Am. Chem. Soc.* **1985**, *107*, 3855. (c) Raven, S. R.; Meyer, T. J. *Inorg. Chem.* **1988**, *27*, 4478.

(3) Kline, M. A.; Barley, M. H.; Meyer, T. J. *Inorg. Chem.* **1987**, *25*, 2197.

(4) (a) Murphy, W. R., Jr.; Takeuchi, K. J.; Barley, M. H.; Meyer, T. J. *Inorg. Chem.* **1986**, *25*, 1041. (b) Thompson, M. S.; Meyer, T. J. *J. Am. Chem. Soc.* **1981**, *103*, 5577. (c) Rhodes, M. R.; Barley, M. H.; Meyer, T. J. Manuscript in preparation.

(5) Ogura, K.; Ishikaw, H. *J. Chem. Soc., Faraday Trans.* **1984**, *80*, 2243-53.

0020-1669/91/1330-0629$02.50/0

transfer reactions occur, (2) to establish the mechanistic details of the individual steps, and, hopefully, (3) to apply the mechanistic insight to problems in chemical catalysis or to the design of models for enzymatic sites that carry out the same or related reactions.

Earlier, it was shown that the nitrite ion can be reduced to ammonia when bound as a ligand in polypyridyl complexes of Ru(II) or Os(II).[4] These reactions occur through a series of sequential, stepwise reactions following the initial acid–base conversion of nitrite into nitrosyl. Coordination complexes of iron(II) have been shown to act as electrocatalysts for the reduction of NO through intermediate nitrosyl formation.[5] Water-soluble iron porphines are electrocatalysts for the reduction of nitrite.[6] This is a significant observation given the fact that the active sites of the nitrite reductase enzymes are known to be heme based.[7]

In this paper, we expand upon the results of an earlier study. It was based on the utilization of edta complexes of Fe(II) or Ru(II) as electrocatalysts for the reduction of nitrite.[8]

Experimental Section

Materials. Iron(II) sulfate heptahydrate, phthalic acid, tetraethylammonium hydroxide, disodium dihydrogen ethylenediaminetetraacetate and hexafluorophosphoric acid (60 wt %) were purchased from Aldrich Chemical Co. and were used without further purification. Potassium dihydrogen phosphate and concentrated phosphoric acid were used as obtained from Fisher Scientific. $[Ru^{III}(Hedta)(H_2O)]$ was prepared by using a literature procedure.[9]

$[Fe^{II}(Hedta)(NO^{\bullet})]^-$. Our procedure was based on one that had been reported previously.[10] A sample of 1.49 g of $Na_2H_2edta{\cdot}2H_2O$ was dissolved in 100 mL of H_2O to yield a solution 40.0 mM in H_2edta^{2-}. A 40-mL aliquot of this solution was placed in a round-bottom flask, which was sealed with a septum. The solution was deaerated by N_2 bubbling for 45 min. A 309.8-mg sample of $FeSO_4{\cdot}7H_2O$ was placed in a second round-bottom flask with a magnetic stirring bar, the flask was sealed and N_2 deaerated. A 28.0-mL aliquot of the H_2edta^{2-} solution was transferred to the flask containing the iron salt by using a deaerated syringe. If the oxygen-free conditions were maintained, the resulting solution containing $[Fe^{II}(Hedta)(H_2O)]^-$ was colorless. Exposure to air resulted in a pale yellow solution. The solution containing $[Fe^{II}(Hedta)H_2O]^-$ was bubbled with NO gas for 1–2 min during which time it turned dark green. Longer reaction times led to a reversal of the color change, possibly due to reoxidation of the product by trace NO_2 in the NO gas stream. The UV/vis spectrum of this solution was consistent with the solution containing 40 mM $[Fe^{II}(Hedta)(NO^{\bullet})]^-$. Electrochemical experiments were performed by syringing aliquots of this stock solution directly into dearated electrochemical cells containing appropriate buffer solutions. UV/vis data in H_2O: λ_{max}, nm (log ϵ) = 209 (3.72), 434 (2.59), 636 (1.83). IR data in H_2O: ν(NO) = 1785 cm^{-1}.

$[Ru^{II}(Hedta)(NO^{+})]$. The compound $[Ru^{II}(Hedta)(NO^{+})]$ was prepared by the reaction between $[Ru^{III}(Hedta)(H_2O)]$ and NO. A solution consisting of 802.8 mg of $[Ru^{III}(Hedta)(H_2O)]$ dissolved in 10 mL of H_2O in a round-bottom flask was prepared. The flask was sealed with a septum and deaerated with Ar for 20 min, NO for 35 min, and Ar again for another 20 min. Pale pink crystals formed after the solution was allowed to sit overnight. The solution was cooled in an ice batch, and 168.2 mg of purple solid was collected by suction filtration and washed with MeOH and Et_2O before drying under vacuum. Extending the reaction time under the NO atmosphere led to the appearance of an additional orange product. The purple compound exhibited ν(CO) bands in the IR region at 1626, 1673, 1743 cm^{-1} and ν(NO) at 1894 cm^{-1}. For the orange compound, bands appeared at 1605, 1735, and 1872 cm^{-1} in addition to the peaks due to the purple compound. The starting compound, $[Ru^{III}(Hedta)(H_2O)]$, was slightly contaminated with Cl^-. Elemental analyses show that the Cl^- content of the purple compound was negligible. Anal. Calcd for $[Ru(Hedta)(NO)]{\cdot}2H_2O$: C, 26.30; H, 3.73; N, 9.20; Cl, 0. Found: C, 26.81; H, 3.46; N, 9.24; Cl, 0.47.

Electrochemical Apparatus. Differential-pulse polarographic experiments were performed on a PAR 174 instrument. Cyclic voltammetry and controlled potential electrolyses were obtained by using a PAR 173 instrument outfitted with a PAR 179 digital readout and an in-house designed wave-form generator. Cells used for cyclic voltammetry and differential-pulse polarography were simple one-compartment cells that utilized a sodium chloride saturated calomel reference electrode (SSCE) and a platinum auxillary. The cell used for bulk electrolyses was a two-compartment gastight cell of homemade design. The auxillary compartment was separated from a mercury-pool working electrode by porous Vycor glass. The cell was outfitted with a gas inlet and outlet. A U-tube manometer hookup was used for equalization of internal and external pressure during sampling of the cell atmosphere. The cell design also included a provision for a glassy-carbon electrode, which was used to obtain cyclic voltammograms during electrolyses. Buffer solutions for controlled-potential electrolyses at pH = 2 were 0.5 M in H_3PO_4 and 0.25 M in $[Et_4N](OH)$ and were formed from 1.0 M H_3PO_4 and 60 wt % $[NEt_4](OH)$ in H_2O (=1.4 M). Buffer solutions at pH = 5 were 0.4 M in phthalic acid and 0.2 M in $[NEt_4](OH)$. In typical electrolysis experiments, 20 mL of the buffer solutions were used. Nitrite ion was added as 500-μL aliquots of a KNO_2 solution prepared by dissolving approximately 350 mg of KNO_2 in 10 mL of H_2O. The use of KNO_2 and $[NEt_4](OH)$ was required in experiments involving the analysis of NH_2OH and NH_3 due to interference of other cations during ion chromatography. The K^+ ion was present at 10 mM in the controlled-potential electrolysis experiments, which minimized its interference. The cation NEt_4^+ was removed from solution by precipitation as its PF_6^- salt following addition of HPF_6 before the analyses were performed.

Methods of Analysis for NH_2OH and NH_3. Analyses for NH_2OH and NH_3 were accomplished by using ion-exchange chromatography on a Dionex Model 2000i ion chromatograph. The analyses involved the workup of the pH = 5 electrolysis solutions in the following manner. A volume of 10 mL of the electrolysis solution was diluted to approximately 19.5 mL and concentrated HPF_6 was added (~0.5 mL required) until the solution pH was 1.5–2.0 as determined with pH paper. The solution was suction filtered into a dry filter flask without washings to remove the precipitated $[NEt_4](PF_6)$. The filtrate was then injected into the ion chromatograph for analysis. For the pH = 2 solutions, the lower NEt_4^+ concentration required less HPF_6. These samples were diluted to ~19.8 mL, and HPF_6 was added until the pH reached 1.5. Again, filtration was required before Dionex analysis. Concentrations of NH_3OH^+ and NH_4^+ were determined by using an HPIC-CS2 column eluted with 30 mM H_3PO_4 and 30 μM Cu_2SO_4. Concentrations determined by this method were accurate to within 0.5 mM, as shown by appropriate blanks. The ion $N_2H_5^+$ could also be determined by using this method although with less accuracy (±1 mM). Hydrazine was not observed as a product in these experiments.

Methods of Analysis for N_2O and N_2. All GC analyses were performed with a Hewlett-Packard Model 5890A gas chromatograph equipped with a thermal conductivity detector and a strip-chart recorder. Gas samples were obtained by using a Hamilton 500-μL gastight syringe and immediately transferred to the GC to minimize contamination of the sample. Analyses for N_2O were obtained by using a Poropak Q column (Alltech Associates) at room temperature. Retention times of 1.5–2.0 min were typical. Analyses for N_2 were performed on a 5A molecular sieve column (Alltech Associates) at room temperature. Retention times and peak shapes were dependent on the activity of the molecular sieves in the column. Typical retention times were 3–5 min. Analyses for N_2 were performed both during and after the electrolyses in order to account for residual atmospheric N_2 in the cell before the experiment. Cell leakage was tested on two separate occasions and found to be minimal for 2–4 h. The reproducibility of the analyses was improved by purging the syringe vigorously prior to sampling and by taking slightly larger samples than needed followed by purging the syringe needle with the excess immediately prior to injection. Both columns were calibrated individually for each experiment.

Results

Nitrosyl Complexes in Solution. The complex $[Fe^{II}(Hedta)(NO^{\bullet})]^-$ was formed and characterized in solution. The stoichiometry of its formation from the corresponding aqua complex and HONO, eq 1, was verified by monitoring the absorption spectrum of a solution containing $[Fe^{II}(Hedta)(H_2O)]^-$ at pH 1.4 as a function of increasing HONO. During the experiment, the initial spectrum of $[Fe^{II}(Hedta)(H_2O)]^+$ changed to a spectrum consistent with the formation of $[Fe^{II}(Hedta)(NO^{\bullet})]^-$ and

(6) (a) Barley, M. H.; Takeuchi, K. J.; Meyer, T. J. *J. Am. Chem. Soc.* **1986**, *108*, 5876. (b) Barley, M. H.; Takeuchi, K. J.; Murphy, W. R., Jr.; Meyer, T. J. *J. Chem. Soc., Chem. Commun.* **1985**, 507. (c) Barley, M. H.; Rhodes, M. R.; Meyer, T. J. *Inorg. Chem.* **1987**, *26*, 1746.
(7) (a) Fernandes, J. B.; Feng, D.; Chang, A.; Keyser, A.; Ryan, M. D. *Inorg. Chem.* **1986**, *25*, 2606–10. (b) Fujita, E.; Fajer, J. *J. Am. Chem. Soc.* **1983**, *105*, 6743–5. (c) Kim, C. H.; Hollocher, T. C. *J. Biol. Chem.* **1983**, *258*, 4861–3. (d) Hanson, L. K.; Chang, C. K.; Davis, M. S.; Fajer, J. *Electron Transp. Oxygen Util. [Int. Symp. Interact. Iron Proteins Oxygen Electron Transp.]* **1982**, 245–52. (e) Hucklesby, D. P.; Cammack, R.; Hewitt, E. J. *Long Ashton Symp. [Proc.]* **1977**, *6* (Nitrogen Assimilation Plants), 245–54.
(8) Rhodes, M. R.; Meyer, T. J. *Inorg. Chem.* **1988**, *27*, 4772–4.
(9) Mukaida, M.; Okuno, H.; Ishimore, T. *Nippon Kagaku Sasski* **1965**, *86*, 598.
(10) Hishinuma, Y.; Kaji, R.; Akimoto, H.; Nakajima, F.; Mori, T.; Kamo, T.; Arikawa, Y.; Nozawa, S. *Bull. Chem. Soc. Jpn.* **1979**, *52*, 2863–5.

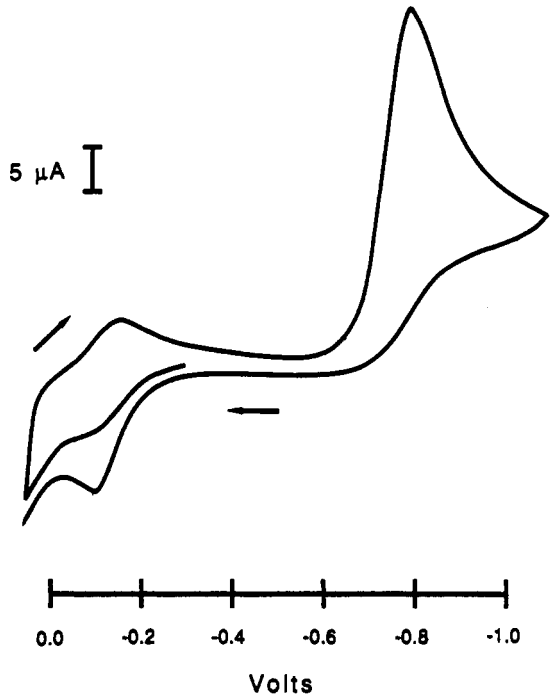

Figure 1. Cyclic voltammogram of $[Fe^{II}(Hedta)(NO^{\bullet})]^-$ (1.0 mM) in 0.1 M KH_2PO_4, 0.1 M H_2SO_4 at pH = 4.0. Scan rate = 100 mV/s at a hanging Hg drop electrode vs SSCE.

$[Fe^{III}(Hedta)(H_2O)]^0$ in equal amounts. The $[Fe^{II}(Hedta)(NO^{\bullet})]^-$ ion has a prominent absorption band at 434 nm. The absorbance at 434 nm increased linearly with [HONO] and leveled off at [HONO] = $^1/_2$[$[Fe^{II}(Hedta)(H_2O)]^-$] in agreement with earlier results.[11] The kinetics of formation of $[Fe^{II}(Hedta)(NO^{\bullet})]^-$ in acidic solutions containing $[Fe^{II}(Hedta)(H_2O)]^-$, HONO, and NO_2^- were reported in a recent paper.[12]

$$2[Fe^{II}(Hedta)(H_2O)]^- + HONO + H^+ \rightarrow [Fe^{III}(Hedta)(H_2O)]^0 + [Fe^{II}(Hedta)(NO^{\bullet})]^- + 2H_2O \quad (1)$$

The assignment of oxidation states implied by the formula $[M^{II}(edta)(NO)]^{2-}$ (M = Fe, Ru) is somewhat arbitrary. We have no direct insight into the detailed electronic structures of these complexes.[15]

For the electrochemical experiments, $[Fe^{II}(Hedta)(NO^{\bullet})]^-$ was prepared *in situ* by bubbling NO gas through a solution containing the iron complex for approximately 1 min. The formation of the nitrosyl was rapid, eq 2, and quantitative as shown by spectro-

$$[Fe^{II}(Hedta)(H_2O)]^- + NO \rightarrow [Fe^{II}(Hedta)(NO^{\bullet})]^- + H_2O \quad (2)$$

photometric measurements.[13] The nitrosyl complex is stable for extended periods in oxygen-free solutions. Exposure to air causes the dark green color of $[Fe^{II}(Hedta)(NO^{\bullet})]^-$ to be replaced by the yellow color of $[Fe^{III}(edta)(H_2O)]^-$. This transformation presumably occurs via oxidation followed by aquation.

Experiments with $[Ru(Hedta)(NO)]^0$ utilized solid samples of the complex. As isolated, the complex contained the singly protonated, five-coordinated edta ligand.

At pH 5.6, the precursor, aqua complex of Ru(III) is deprotonated. At this pH, a reaction occurs between this complex and NO_2^- to give $[Ru^{II}(edta)(NO)]^{2-}$ and $[(edta)Ru^{IV}ORu^{III}(edta)]^{3-}$. The reaction stoichiometry shown in eq 3 was established by cyclic voltammetry.[14]

$$2H^+ + 3[Ru^{III}(edta)(OH)]^{2-} + NO_2^- \rightarrow [Ru^{II}(edta)(NO)]^{2-} + 3H_2O + [(edta)Ru^{IV}ORu^{III}(edta)]^{3-} \quad (3)$$

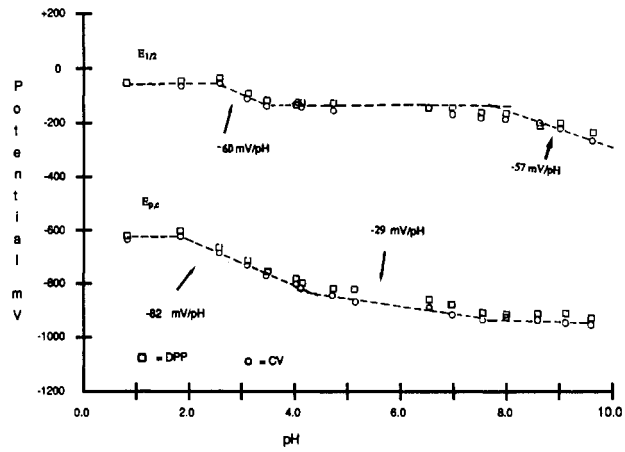

Figure 2. Potential–pH diagrams for $[Fe(Hedta)(NO^{\bullet})]^-$ in 0.1 M KH_2PO_4 adjusted to the desired pH by using either 1.0 M H_2SO_4 or 0.5 M NaOH. Data obtained by cyclic voltammetry at a scan rate of 100 mV/s are shown as circles and data obtained by differential-pulse polarography at 10 mV/s, pulse height 10 mV, are shown as squares. The dashed lines are an attempt to construct linear regions based on the cyclic voltammetric data.

Electrochemistry of $[Fe(Hedta)(NO^{\bullet})]^-$. pH Dependence. A cyclic voltammogram of $[Fe(Hedta)(NO^{\bullet})]^-$ at a hanging Hg drop electrode at pH = 4.0 is shown in Figure 1. An initial oxidative scan gave a well-defined, chemically reversible wave at $E_{1/2}$ = −0.12 V (ΔE_p = 65 mV at 100 mV/s) for the $Fe(NO^+)/Fe(NO^{\bullet})$ couple. The appearance of pH-dependent oxidative and reductive adsorption waves, at +0.09 V and 0.05 mV, respectively, at pH = 4.0 (not shown), are a complicating feature at Hg. At glassy carbon, the electron-transfer kinetics for the $Fe(NO^+)/Fe(NO^{\bullet})$ couple were slow with ΔE_p = 360 mV at 100 mV/s. At more negative potentials, a multielectron, irreversible reduction wave appeared at $E_{p,c}$ = −0.81 V, at pH = 4.0.

Both waves in Figure 1 are pH dependent. The variations in $E_{1/2}$ or $E_{p,c}$ with pH are shown in Figure 2. Also shown are peak potentials obtained by differential-pulse polarography. For the $Fe(NO^+)/Fe(NO^{\bullet})$ wave three breaks appear in the $E_{1/2}$–pH profile. The first two occur at pH = ∼2.6 and ∼3.2. A line having a slope of ∼60 mV/pH unit is shown drawn through the data in this region. The third break is less well-defined and occurs in the range pH = 6.3–8.5. The first break is close to the pK_a for the uncoordinated carboxylate arm of $[Fe^{II}(Hedta)(H_2O)]^-$ (pK_a = 2.06).[16-18] The pK_a for HONO is 3.35, but since we are observing the nitrosyl complex, this equilibrium presumably has no effect on the measured potentials. Between pH = 8 and pH = 10, an additional, small, pH-independent wave appeared at ∼−90 mV (not shown). Its prominence increased at slow scan rates.

The pH dependence for the irreversible reduction is even more complex. In the plot of $E_{p,c}$ vs pH in Figure 2, lines drawn through the experimental points have slopes of ∼−82 mV/pH unit (1.8 < pH < 4.4), ∼−28 mV/pH unit (4.4 < pH < 7.6) and ∼−14 mV/pH unit (pH > 7.6). Above pH = 8.5, additional, small reduction waves appear in the cyclic voltammograms. At pH = 9.1, these waves appear at E_p = −700, −1000, and −1090 mV.

Electrochemistry of $[Ru^{II}(Hedta)(NO^+)]^0$. pH Dependence. The NO group in $[Ru^{II}(Hedta)(NO^+)]^0$ is strongly bound and nonlabile. In a formal sense, it can be viewed as bound NO^+.[15] In Figure 3 are shown representative cyclic voltammograms of solutions containing this complex obtained at Hg at different pH values. The reduction of $[Ru^{II}(Hedta)(NO^+)]^0$ to $[Ru^{II}(Hedta)(NO^{\bullet})]^-$ occurs at $E_{1/2}$ = −0.34 V (ΔE_p = 70 mV) at pH =

(11) Uchiyama, S.; Nozaki, K.; Muto, G. *Bunseki Kagaku* **1977**, *26*, 219.
(12) Zang, V.; Kotowski, M.; van Eldik, R. *Inorg. Chem.* **1988**, *27*, 3249–83.
(13) Hishinuma, Y.; Kaji, R.; Akimoto, H.; Nakajima, F.; Mori, T.; Kamo, T.; Arikawa, Y.; Nozawa, S. *Bull. Chem. Soc. Jpn.* **1979**, *52*, 2863–5.
(14) Baar, R. B.; Anson, F. C. *J. Electroanal. Chem. Interfacial Electrochem.* **1985**, *187*, 265–82.
(15) (a) McCleverty, J. A. *Chem. Rev.* **1979**, *79*, 53–76. (b) Enemark, J. H.; Feltham, R. D. *Coord. Chem. Rev.* **1974**, *13*, 339.
(16) Clark, N. H.; Martell, A. E. *Inorg. Chem.* **1988**, *27*, 1297–8.
(17) Gustafson, R. L.; Martell, A. E. *J. Phys. Chem.* **1963**, *67*, 576.
(18) Schwarzenbach, G.; Heller, J. *Helv. Chim. Acta* **1951**, *34*, 576.

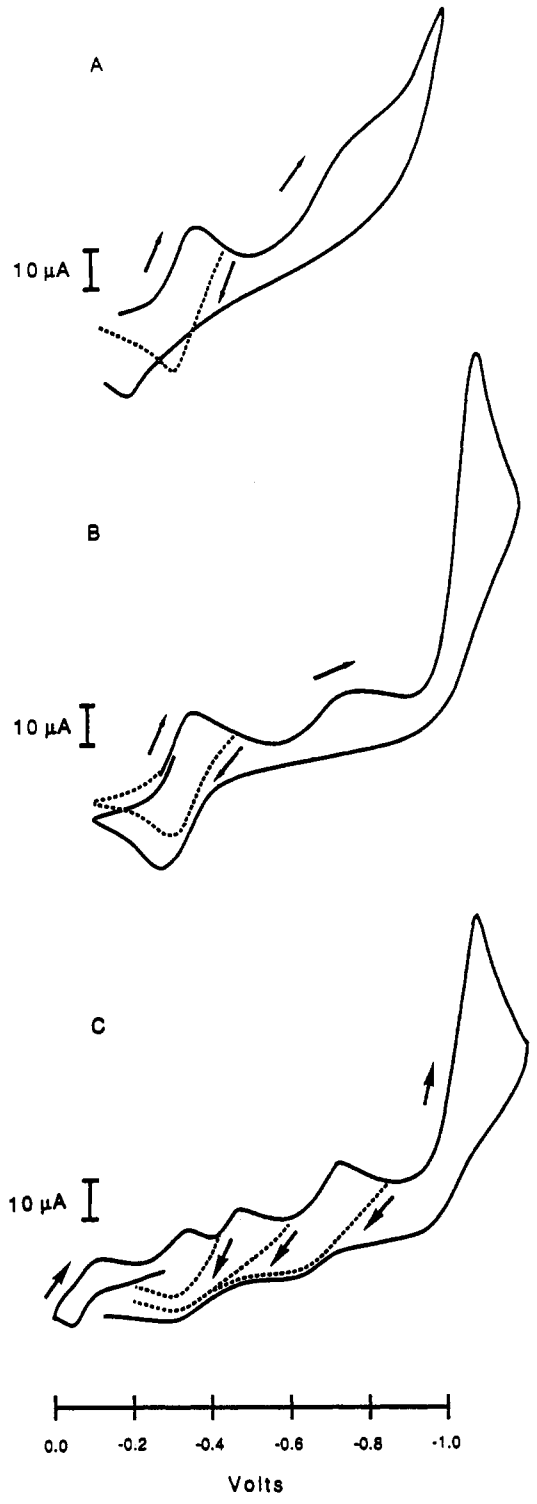

Figure 3. Cyclic voltammograms of $[Ru^{II}(Hedta)(NO^+)]^0$ (1.0 mM) at (A) pH = 4.93, (B) pH = 7.51, and (C) pH = 10.48. Buffer solutions were prepared from 0.1 M KH_2PO_4 by adding 1.0 M H_2SO_4 or 0.5 M NaOH. Scan rate = 100 mV/s at a hanging Hg drop electrode vs SSCE.

4.9. This wave is more nearly electrochemically reversible at Hg than at glassy carbon. It is followed by an irreversible, multielectron reduction at $E_p = -0.75$ V. After the scan through the multielectron reduction, the oxidative component of the $[Ru^{III/II}(edta)H_2O]^{-/2-}$ couple was observed at −0.18 V. Additional waves appear in differential pulse polarograms at $E_p = -0.87$ and −1.10 V which are pH independent from pH = 2 to pH = 6.

Variations in $E_{1/2}$ with pH for the first reduction or of $E_{p,c}$ for the second and third reductions are shown in Figure 4. The variations in peak potentials from differential-pulse polarograms with pH are also shown. For the first reduction wave, there was

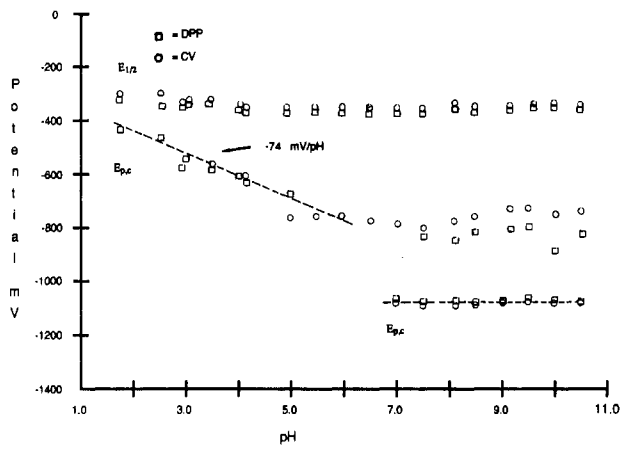

Figure 4. Potential–pH diagram for $[Ru(Hedta)(NO^+)]^0$. Conditions are as in Figure 2 except that for the differential-pulse polarograms (squares) the scan rate was 5 mV/s and the pulse height was 5 mV.

a slight decrease in $E_{1/2}$ with pH (~−12 mV/pH unit) below pH = 4. For the second reduction, $E_{p,c}$ decreased by ~74 mV/pH unit from pH = 3 to pH = 5. In the region pH = 5–7, the pH dependence of the second wave was lost and a pH-independent, irreversible wave appeared at −1.09 V. At pH = 10.5, the solution electrochemistry was even more complex, with additional waves appearing at −0.09 and −0.46 V, Figure 3c.

Controlled-Potential Electrolyses. A series of controlled-potential electrolyses were conducted on solutions containing excess NO_2^- in order to test the ability of the edta complexes to act as catalysts for the net electrochemical reduction of NO_2^-. The iron complex was added as the nitrosyl and the ruthenium complex as $[Ru^{III}(Hedta)(H_2O)]$. The potentials and pH values chosen for study were based on the results obtained by cyclic voltammetry. The results of the electrolyses are summarized in Table I both as the percent conversion to a given product and as the percentage of the current passed in forming a particular product.

The catalytic currents increased noticeably as the pH was decreased. At pH ≥ 5.0 the rate of catalysis decreased and the stability of the catalysts fell. By pH = 7, catalysis by the iron complex proceeded through only a few turnovers before dying off. For the ruthenium complex at pH = 7, approximately 30 turnovers occurred before catalytic activity ceased.

The loss of catalytic activity as the pH was raised was not due to the instability of the reduced nitrosyl complexes, $[M^{II}(edta)(NO)]^{2-}$. They remain stable up to pH = 10 or 11 as shown by UV–visible spectra and cyclic voltammetric measurements. The loss of catalytic activity was accompanied by changes in the spectra and electrochemical properties of the complexes. One pathway for loss of catalytic activity may involve *oxidative* decomposition. The evidence for this conclusion is based on the appearance of CO_2 as an electrolysis product for both complexes as the pH was raised. For the ruthenium complex, one to two molecules of CO_2 were observed as a coproduct per catalyst molecule at pH = 5 and three to five molecules at pH = 7 as shown by gas chromatography.

Discussion

In previous studies based on polypyridyl complexes of Ru, it was shown that acid–base equilibria exist between bound nitrosyl and nitro ligands and that the nitrosyl is the active form toward reduction.[4,6,19] For example, for $[Ru(tpy)(bpy)(NO)]^{3+}$ (bpy is 2,2′-bipyridine, tpy = 2,2′:6′,2″-terpyridine) or $[Os(tpy)(bpy)(NO)]^{3+}$, the pH values at which the nitrosyl and nitro forms are present in equal amounts are 2.5 and 8.0, respectively. Either complex can be reduced chemically or electrochemically to the corresponding ammine.

The same pattern of acid–base chemistry and ligand-based reduction appears to exist for the edta complexes, but we have

(19) Pipes, D. W.; Meyer, T. J. *Inorg. Chem.* **1984**, *23*, 2466.

Table I. Product Yields in the Controlled-Potential Reduction of NO_2^-/HONO Catalyzed by $[M^{II}(edta)(H_2O)]^{2-}$ (M = Fe, Ru)[a]

				N-containing products as a % of added NO_2^-/HONO					% of the current used to form the N-containing products[b]				
M^{II}	pH	E_{app}, V[c]	n[d]	N_2O	N_2	NH_3OH^+	NH_3^+	tot.[e]		N_2O	NH_3OH^+	NH_4^+	tot.
Fe	2.1	−0.80	3.0	49	8	49	0	106	36	9	71	0	116
	5.0[f]	−0.90	3.4	16	6	11	8	41	22	13	30	31	95
Ru	2.1	−0.30	2.4	10	6	0	0	15	52	45	0	0	97
		−0.55	3.2	47	17	11	18	97	30	16	14	34	99
		−0.90	3.6	30	4	21	17	72	5	1	7	9	21[g]
	5.0	−0.75	3.9	26 ± 1	15 ± 1	16 ± 5	29 ± 3	86 ± 10	16 ± 1	14 ± 2	20 ± 6	54 ± 5	103 ± 14
		−0.90	2.8	40	19	8	6	73	38	27	15	17	97
	7.2	−1.00	4.5	0	15	0	16	31	0	34	0	72	106

[a] At room temperature. $[NO_2^-]$ = 10 mM and [catalyst] = 0.1 mM. The working electrode was a Hg pool with 12.6 cm^2 area; the electrolyses were continued until the current had fallen to 4% of its initial value. Typical uncertainties are shown in line 6. [b] The % current efficiency for each of the N-containing products was calculated from the formula % current efficiency = $[(m_i n_i F)/Q_t]100\%$, where m_i is the number of moles of product, n_i is the n value for its formation (n = 4 for N_2O, 6 for N_2, 4 for NH_3OH^+, and 6 for NH_4^+), F is the Faraday constant and Q_t is total charge passed in the electrolysis. Hydrazine was not observed as a product within the limits of detection (<10% nitrogen). [c] Applied potential vs. SSCE. [d] n is the average number of electrons added per nitrite ion during the electrolysis. This quantity was calculated as the ratio of electrochemical equivalents passed to total NO_2^-/HONO reduced. [e] This quantity also represents the number of turnovers of catalyst per NO_2^-/HONO reduced. [f] [Fe] = 0.5 mM; the number of tunovers was 8.2. [g] Significant amounts of H_2 were observed by GC.

been able to define it in less detail. For example, we have been unable to obtain quantitative information concerning the nitrosyl–nitro equilibria in eq 4. For M = Fe, $[Fe^{II}(edta)(NO^+)]^-$ is insufficiently stable to estimate a reliable pK value by electrochemical measurements. The fall in catalytic activity for M = Fe at pH ~ 5 may signal the onset of nitrosyl to nitro interconversion for the iron complex. For $[Ru^{II}(edta)(NO^+)]^-$, the

$$[M^{II}(edta)(NO^+)]^- + H_2O \rightleftharpoons [M(edta)(NO_2)]^{3-} + 2H^+ \quad (4)$$

$Ru^{III/II}$ wave for the corresponding aqua couple begins to appear at around pH ~ 9. This suggests that nitrosyl/nitrite interconversion followed by aquation, eqs 5 and 6, may have occurred by this pH.

$$[Ru^{II}(edta)(NO)]^- + 2OH^- \rightarrow [Ru^{II}(edta)(NO_2)]^{3-} + H_2O \quad (5)$$

$$[Ru(edta)(NO_2)]^- + H_2O \rightarrow [Ru^{II}(edta)(H_2O)]^{2-} + NO_2^- \quad (6)$$

The acid–base chemistry is confined to the $M^{II}(NO^+)$ forms of the complexes, at least to pH 11. In the reduced form, $[M(edta)(NO^\bullet)]^{2-}$, the nitrosyl-based reduction waves persist up to pH = 11 for either M = Fe or Ru.

The nitrosyl complexes $[M^{II}(Hedta)(NO^+)]^0$ appear upon reduction of $[M^{III}(Hedta)(H_2O)]^0$ in acidic solutions in the presence of nitrite. Their formation was shown by the appearance of the nitrosyl-based reduction waves in cyclic voltammograms, e.g., Figures 1 and 3. Exhaustive, controlled potential reduction of these solutions gave rise to mixtures of N_2O, N_2, NH_3OH^+, and NH_4^+, the relative amounts of which depended upon the applied potential and the pH (Table I). The potentials of the couples that interrelate nitrite and the lower oxidation states of nitrogen are summarized at pH = 2.0 vs. SSCE in the Latimer diagrams and half-reactions in Scheme I. These potentials show that, even at the most positive potentials used in the electrolyses, electrocatalysis occurs with high overvoltages. The origin of the overvoltage lies in the potential requirements imposed by the onset of the reduction of the nitrosyl complexes.

Scheme I. Reduction Potentials at pH = 2.0 vs SSCE

$$HONO \xrightarrow{+0.93} N_2O \xrightarrow{+1.41} N_2 \xrightarrow{-2.35} NH_3OH^+ \xrightarrow{+1.13} N_2H_5^+ \xrightarrow{+0.85V} NH_4^+$$

$$2HONO + 6H^+ + 6e^- \rightarrow N_2 + 4H_2O \quad +1.09\ V$$

$$HONO + 5H^+ + 4e^- \rightarrow NH_3OH^+ + H_2O \quad +0.23\ V$$

$$2HONO + 11H^+ + 10e^- \rightarrow N_2H_5^+ + 4H_2O \quad +0.41\ V$$

$$HONO + 7H^+ + 6e^- \rightarrow NH_4^+ + 2H_2O \quad +0.49\ V$$

Polypyridyl complexes of Ru and Os give similar product distributions, but they are not *catalysts* for the reactions.[4] In a catalytic sense, the edta complexes have the virtue of substitutional lability. Following the reduction of the M^{III} aqua complexes to M^{II}, nitrosyl complexes form rapidly in solution. Multielectron reduction of the nitrosyls occurs and is followed by ligand loss and aquation. The substitutional step is relatively rapid and completes the catalytic cycle. The individual steps involved in the six-electron reduction of NO_2^- to NH_4^+ are shown in eqs 7–9. Similar reactions can be written for reduction to the intermediate oxidation states N_2O, N_2, or NH_3OH^+.

$$[M^{II}(Hedta)(H_2O)]^- + NO_2^- + 2H^+ \rightarrow [M^{II}(Hedta)(NO)]^0 + H_2O \quad (7)$$

$$[M^{II}(Hedta)(NO)]^0 + 6e^- + 5H^+ \rightarrow [M^{II}(Hedta)(NH_3)]^- + H_2O \quad (8)$$

$$[M^{II}(Hedta)(NH_3)]^- + H^+ + H_2O \rightarrow [M^{II}(Hedta)(H_2O)]^+ + NH_4^+ \quad (9)$$

For the polypyridyl complexes, stoichiometric reduction of the nitrosyls occurs to give the corresponding ammines $[M(tpy)(bpy)(NH_3)]^{2+}$ (M = Ru, Os). If N_2 or N_2O is the product of reduction, the aqua complexes $[M(tpy)(bpy)(H_2O)]^{2+}$ appear as products. Aquation and/or nitrosation of these complexes are too slow for them to be useful as catalysts, at least at room temperature.

The ability of the edta complexes to act as catalysts is restricted to acidic solution. For the complex of Fe(II) this restriction is intrinsic. It arises from the pH-based requirement associated with the nitrosyl/nitro equilibrium in eq 4. Since the nitrosyl complexes are the reactive forms toward reduction, solutions must be sufficiently acidic that the nitrosyl form is present in a kinetically significant amount. For the complex of Ru(II), the pH where the nitro and nitrosyl forms are present in significant amounts may be considerably higher, apparently near pH = 9. There is an additional limitation above pH = 5 for both complexes. As noted in the Results, as the pH is raised, a pathway or pathways appear that lead to the decomposition of the catalysts. Decomposition becomes important for the complex of Fe^{II} above pH 5 and for the complex of Ru^{II} above pH = 7.

In the presence of excess NO_2^-, an additional decomposition pathway exists for $[Ru^{III}(Hedta)H_2O]^0$ as the pH is raised. Under these conditions, the Ru^{III} complex is unstable with respect to the formation of $[Ru^{II}(edta)(NO)]^{2-}$ and $[(edta)RuORu(edta)]^{3-}$, eq 3. This reaction, which occurs rapidly when solutions containing $[Ru^{III}(Hedta)(H_2O)]$ and NO_2^- are mixed, was not observed for $[Fe^{III}(Hedta)(H_2O)]^0$. The spontaneity of the reaction for Ru may be a reflection of a stronger M^{II}–nitrosyl bond and stabilization of the μ-oxo complex by strong electronic coupling across the μ-oxo bridge.[15,20]

The reductions of the nitrosyl complexes have complex pH dependences (Figures 2 and 4). The break in the $E_{1/2}$–pH curve for the $Fe^{II}(NO^+)/Fe^{II}(NO^•)$ couple in acidic solution can be explained by the existence of pH-dependent equilibria involving the uncoordinated edta arm. The couples that may be involved are shown in eqs 10–12. The decrease in $E_{1/2}$ with pH of ~60 mV/pH unit from 2.6 < pH < 4.1 is near the value predicted by the Nernst equation for the gain of a proton in the reduced form of the couple. For the corresponding $Ru^{II}(NO^+)/Ru^{II}(NO^•)$

$$pH < 2.6 \quad [Fe^{II}(Hedta)(NO^+)]^0 + e^- \rightarrow [Fe^{II}(Hedta)(NO^•)]^- \quad (10)$$

$$2.6 < pH < 4.1 \quad [Fe^{II}(edta)(NO^+)]^- + e^- + H^+ \rightarrow [Fe^{II}(Hedta)(NO^•)]^- \quad (11)$$

$$pH > 4.1 \quad [Fe^{II}(edta)(NO^+)]^- + e^- \rightarrow [Fe^{II}(edta)(NO^•)]^{2-} \quad (12)$$

couple, the data in this region are less well-defined. A slight decrease in $E_{1/2}$ with pH does appear from pH = 2 to pH = 4.1. Acid–base equilibria involving the unbound arm of the edta ligand occur in this pH range for the $[Ru^{III/II}(Hedta)(H_2O)]^{0/-}$ couple.[14]

For the $Fe^{II}(NO^+)/Fe^{II}(NO^•)$ couple, an additional, ill-defined break appears in the $E_{1/2}$ vs pH plot in the range pH = 6.3–8.5. This break does not appear for the $Ru^{II}(NO^+)/Ru^{II}(NO^•)$ couple. Its origin is not clear. One possibility is that it could involve deprotonation of bound water in an aqua complex with edta as a tetradentate ligand, eqs 13 and 14.

$$[Fe(edta)(NO)(H_2O)]^- \rightleftharpoons [Fe(edta)(NO)(OH)]^{2-} + H^+ \quad (13)$$

$$[Fe^{II}(edta)(NO)(OH)]^{2-} + e^- + H^+ \rightarrow [Fe^{II}(edta)(NO^•)(OH)]^{2-} \quad (14)$$

For $[Ru^{II}(edta)(NO^+)]^-$, two additional reduction waves appear past the $Ru^{II}(NO)/Ru^{II}(NO^•)$ couple, Figures 3 and 4. A pattern of three reduction waves has also been found for $[Ru(tpy)(bpy)(NO)]^{3+}$.[4a] By a comparison of integrated peak areas, the second reduction also appears to be a one-electron process leading to an overall two-electron reduction past the second wave. For the polypyridyl complexes, reduction to the two-electron stage has been interpreted as leading to intermediates that contain either the $M(NO^-)$ or M(NHO) groups, depending upon the pH. If the chemistry is the same, the break in the $E_{p,c}$–pH curve in Figure 4 at pH ~ 5.5 may signal that the pK_a for the reduced complex $[Ru(edta)(NHO)]^{2-}$ has been reached. If so, the two couples that are involved are shown in eq 15.

$$[Ru^{II}(edta)(NO^•)]^{2-} + e^- + H^+ \rightarrow [Ru(edta)(NHO)]^{2-} \quad (15a)$$

$$[Ru^{II}(edta)(NO^•)]^{2-} + e^- \rightarrow [Ru(edta)(NO)]^{3-} \quad (15b)$$

The second reduction is followed by an irreversible, multielectron reduction wave at −1.09 V. This wave, which is masked by the background in acidic solution, is pH independent from pH = 7 to pH = 10.5, Figure 4. The additional waves that appear at −0.09 and −0.46 V in the cyclic voltammogram in Figure 3c at pH = 10.5 are attributable to the $[Ru^{III}(edta)(OH)]^{2-}/[Ru^{II}(edta)(H_2O)]^{2-}$ and $[(edta)Ru^{IV}–O–Ru^{III}(edta)]^{3-/4-}$ couples.[22] The appearance of these products suggests that when the complex is allowed to stand, either NO is lost from $[Ru^{II}(edta)(NO^+)]^-$ or that, at this pH, the nitrosyl complex is being converted into $[Ru^{II}(edta)(NO_2)]^{3-}$ and then aquates. The mixed-valence complex is known to form spontaneously at high pH in the presence of O_2.[22]

For the iron complex, an irreversible, multielectron reduction wave appears in acidic solution at −0.62 V. Because of its shift to more positive potentials compared to Ru, it probably overlaps and incorporates the second one-electron reduction observed for the complex of Ru. The multielectron nature of the wave was demonstrated by comparing relative peak currents for the irreversible reduction and the one-electron $Fe^{II}(NO^+)/Fe^{II}(NO^•)$ couple. The area of this peak was 2.6 times that of the one-electron couple at pH = 4.0.

The multielectron wave is pH-dependent, Figure 2. This is to be expected given the proton demands of the reactions that lead to the products of the electrolyses, eqs 16–19. Although the

$$2[Fe^{II}(edta)(NO^•)]^2 + 2e^- + 2H^+ + H_2O \rightarrow 2[Fe^{II}(edta)(H_2O)]^{2-} + N_2O \quad (16)$$

$$2[Fe^{II}(edta)(NO^•)]^{2-} + 4e^- + 4H^+ \rightarrow 2[Fe^{II}(edta)(H_2O)]^{2-} + N_2 \quad (17)$$

$$[Fe^{II}(edta)(NO^•)]^{2-} + 3e^- + 4H^+ + H_2O \rightarrow [Fe^{II}(edta)(H_2O)]^{2-} + NH_3OH^+ \quad (18)$$

$$[Fe^{II}(edta)(NO^•)]^{2-} + 5e^- + 6H^+ + H_2O \rightarrow [Fe^{II}(edta)(H_2O)]^{2-} + NH_4^+ \quad (19)$$

irreversible nature of the electrochemical process(es) precludes a quantitative analysis of the $E_{p,c}$–pH data, some inferences can be drawn. Reduction to products such as N_2O or NH_3OH^+ requires the addition of both protons and electrons. The decrease in $E_{p,c}$ with pH from pH = 2 to pH = 4 is consistent with the addition of both protons and electrons during the voltammetric sweep. As the pH is raised, the pH dependence of $E_{p,c}$ falls. Between pH = 4.4 and pH = 7.6 the slope is ~−28 mV/pH unit. This corresponds to a process or processes in which the ratio of electrons to proton is ~2. At pH = 5.0, N_2O, N_2, NH_3OH^+, and NH_4^+ are all observed as products of the electrolyses. These observations, when taken with the proton requirements in eqs 16–19, place certain demands on the mechanism. If the fully reduced products appear during a single reductive sweep, the addition of electrons at the electrode must be followed by the accumulation of additional protons in rapid steps that follow. It is also conceivable that initial reduction at the electrode gives intermediates that are pseudostable and evolve into the final products after the electrode reaction is complete. Evidence for such intermediates has been found in the reduction of polypyridyl–nitrosyl complexes of Ru and Os by cyclic voltammetry.[4] However, there is no evidence for waves arising from analogous intermediates on reverse, oxidative scans for either edta complex.

Mechanism of NO_2^- Reduction. On the basis of our results, there is at least a superficial resemblance between the mechanisms for nitrite reduction by the edta complexes and those found earlier for polypyridyl complexes of Ru or Os[4] and for water-soluble iron porphines.[6] The first step involves formation of a nitrosyl complex, eq 20. In this step, initial nitrite binding may occur, eq 21,

$$M^{II}(H_2O) + NO_2^- + 2H^+ \rightarrow [M^{II}(NO^+)]^+ + H_2O \quad (pH < 7) \quad (20a)$$

$$M^{II}(H_2O) + NO_2^- + H_2O \rightarrow [M^{II}(NO^+)]^+ + 2OH^- \quad (pH > 7) \quad (20b)$$

$$[M^{II}(edta)(H_2O)]^{2-} + NO_2^- \rightarrow [M^{II}(edta)(NO_2)]^{3-} + H_2O \quad (21)$$

$$[M^{II}(edta)(NO_2)]^{3-} + 2H^+ \rightarrow [M^{II}(edta)(NO^+)]^- + H_2O \quad (M = Fe) \quad (22a)$$

$$[M^{II}(edta)(NO_2)]^{3-} + H_2O \rightarrow [M^{II}(edta)(NO^+)]^- + 2OH^- \quad (M = Ru;\ pH > 7) \quad (22b)$$

(20) (a) Weaver, T. R.; Meyer, T. J.; Adeyemi, S. A.; Brown, G. M.; Eckberg, R. P.; Hatfield, W. E.; Johnson, E. C.; Murray, R. W.; Untereker, D. *J. Am. Chem. Soc.* **1975**, *97*, 3039. (b) Burchfield, D. E.; Richman, R. M. *Inorg. Chem.* **1985**, *24*, 852–7.

(21) (a) Lopez-Alcala, J. M.; Puerta-Vizcaino, M. C.; Gonzalez-Vilchez, F.; Duesler, E. N.; Tapscott, R. E. *Acta Crystallogr., Sect. C: Cryst. Struct. Commun.* **1984**, *C40*, 939–41. (b) Nesterova, Y. M.; Polynova, T. N.; Porai-Koshits, M. A. *Koord. Khim.* **1975**, *1*, 966–74. (c) Solans, X.; Font Altaba, M.; Garcia-Oricain, J. *Acta Crystallogr., Sect. C.: Cryst. Struct. Commun.* **1984**, *C40*, 635–8.

(22) Shimizu, K.; Matsubara, T.; Sato, G. P. *Bull. Chem. Soc. Jpn.* **1974**, *47*, 1651.

followed by acid–base interconversion to nitrosyl. The separate steps are clearly identifiable for polypyridyl complexes of Ru and Os.[4] Other pathways are available for the formation of the nitrosyls, one, for example, involving initial oxidation followed by nitrosyl formation.[12]

$$M^{II}(H_2O) + NO_2^- + 2H^+ \rightarrow M^{III}(H_2O)^+ + NO + H_2O$$

$$M^{III}(H_2O)^+ + NO \rightarrow M^{II}(NO^+)$$

From the electrochemical results, acid–base interconversion may occur at pH ~ 9 for M = Ru and at pH ~ 5 from M = Fe.

Dehydration of nitrite to give nitrosyl creates a low-lying acceptor orbital that is largely $\pi^*(NO)$ in character. As formed for the polypyridyl complexes of Ru and Os, the initial one-electron reduction of the nitrosyl complexes may occur at this orbital, eq 23. The first reductions of $[M^{II}(Hedta)(NO^+)]^0$ or $[M^{II}(edta)(NO^+)]^-$ occur at potentials that are ~200 mV more positive for M = Fe than for M = Ru. From this result it can be inferred that there is more NO^+ character and less $d\pi \rightarrow \pi^*(NO)$ back-bonding for the iron complex. This is an expected result given the greater $d\pi$ orbital extension for Ru. By contrast, the second reduction for M = Fe is shifted to considerably more negative potentials than for M = Ru. Above pH 5, the second reduction for Ru is pH independent and appears at a potential ~500 mV more negative than the first reduction. For M = Fe at pH = 5, a discrete, second wave is not observed before the appearance of the multielectron wave at −0.87 V. Here, the difference in potentials between the first and second reductions is >800 mV.

$$[M^{II}(edta)(NO^+)]^- + e^- \rightarrow [M^{II}(edta)(NO^\bullet)]^{2-} \quad (23)$$

The one-electron reduction product $[Fe^{II}(edta)(NO^\bullet)]^{2-}$ is stable toward the formation of N_2O and N_2 but $[Ru^{II}(edta)(NO^\bullet)]^{2-}$ is not. Controlled-potential electrolysis of acidic solutions containing the Ru complex past the first reduction wave at −0.30 V led to N_2 and N_2O. The reduction at −0.30 V proceeded at a current level that was lower by a factor of 10 than reduction at the irreversible wave at −0.55 V. The difference in behavior between the Fe and Ru complexes lies in the potential differences between their first and second reductions. At pH = 2, the potential difference was 120 mV for M = Ru and 560 mV for M = Fe. Because the potential difference is small for M = Ru, a pathway exists for multielectron reduction following the addition of one electron. It involves initial disproportionation, eq 24, followed by coupling to give N_2O or further reduction to give N_2, eqs 25 and 26. These reactions are written by assuming that the unbound edta arm is protonated at pH = 2. Qualitative observations show that the stability of the one-electron reduced complex for M = Ru is enhanced as the pH is raised and the difference between the first and second reductions increase, as expected.

$$2[Ru^{II}(Hedta)(NO^\bullet)]^- + H^+ \rightarrow [Ru^{II}(Hedta)(NO^+)]^0 + [Ru(Hedta)(NHO)]^- \quad (24)$$

$$2[Ru(Hedta)(NHO)]^- + H_2O \rightarrow 2[Ru^{II}(Hedta)(H_2O)]^- + N_2O \quad (25)$$

$$2[Ru(Hedta)(NHO)]^- + 2H^+ + 2e^- \rightarrow 2[Ru^{II}(Hedta)(H_2O)]^- + N_2 \quad (26)$$

For M = Ru a second, discrete one-electron reduction is observed. If the resulting two-electron-reduced intermediate is $[Ru(edta)(NO)]^{3-}$ or $[Ru(edta)(NHO)]^{2-}$, as suggested by the pH-dependence data, the appearance of N_2O as a product can be explained by N–N coupling, eq 25. Reduction past the n = 2 stage gave more highly reduced products as well. In order to explain this result, it may be necessary to invoke disproportionation reactions such as the one shown in eq 27.

$$2[M(Hedta)(NHO)]^- + H^+ \rightarrow [M^{II}(Hedta)(NO^+)]^0 + [M^{II}(Hedta)(NH_2OH)]^- \quad (27)$$

For M = Ru, further reduction occurs at a third wave. With the addition of a third electron, the formation of N_2 occurs, perhaps by N–N coupling as shown in eq 26. Both NH_3OH^+ and NH_4^+ also appear as products at this potential. They may appear via two-electron transfer and formation of hydroxylamine, eq 28. In

$$[M(edta)(NHO)]^{2-} + 2e^- + 2H^+ \rightarrow [M^{II}(edta)(NH_2OH)]^- + H^+ \rightarrow [M^{II}(Hedta)(H_2O)]^- + NH_3OH^+ \quad (28)$$

the electrocatalytic reduction of NO_2^- by water-soluble iron porphines, NH_3OH^+ appears as a precursor to NH_4^+. It builds up as an intermediate in acidic solution because it is protonated (pK_a = 6.03 for NH_3OH^+). This hinders coordination and further reduction to NH_3/NH_4^+.

Acknowledgment is made to the National Institutes of Health for support of this work under Grant No. 5-R01-GM32296-06.